EFDA–JET–PR(08)32

I.T. Chapman, C.G. Gimblett, M.P. Gryaznevich, T.C. Hender,
D.F. Howell, Y.Q. Liu, S.D. Pinches and JET EFDA contributors

Stability of the Resistive Wall Mode in JET

Stability of the Resistive Wall Mode in JET

I.T. Chapman[1], C.G. Gimblett[1], M.P. Gryaznevich[1], T.C. Hender[1], D.F. Howell[1], Y.Q. Liu[1], S.D. Pinches[1] and JET EFDA contributors*

JET-EFDA, Culham Science Centre, OX14 3DB, Abingdon, UK

[1]EURATOM-UKAEA Fusion Association, Culham Science Centre, OX14 3DB, Abingdon, OXON, UK
** See annex of F. Romanelli et al, "Overview of JET Results", (Proc. 22 [nd] IAEA Fusion Energy Conference, Geneva, Switzerland (2008)).*

Preprint of Paper to be submitted for publication in
Plasma Physics and Controlled Fusion

ABSTRACT.
The kinetic effects influencing the stability of the Resistive Wall Mode (RWM) are investigated by applying a drift kinetic code to calculate the change in the potential energy of the mode in the presence of thermal and energetic particles. The analysis is carried out for typical JET high- plasmas. It is found that the strongest kinetic damping of the RWM arises due to mode resonance with the precession motion of the trapped thermal particles. The stability of the RWM in JET plasmas is also probed by using active MHD spectroscopy. The frequency spectrum of the plasma response to oscillating externally applied fields has been measured and fitted to parameter models in order to infer the stability of the RWM. A new model retaining information about the plasma response is presented to describe the resonant field amplification in the presence of a stable RWM and favourably compared with the calculated response.

1. INTRODUCTION

The ultimate performance limit in advanced tokamak scenario operation is often set by the Resistive Wall Mode (RWM). The RWM is a macroscopic pressure-driven kink mode, whose stability is mainly determined by damping arising from the relative rotation between the fast rotating plasma and the slowly rotating wall mode. In the absence of a surrounding wall, the plasma is stable to kink modes until the normalised plasma pressure, $\beta = 2\mu\langle p\rangle/B^2$, exceeds a critical value, β_∞. In the presence of an ideally conducting wall, the plasma is stable to a critical value, β_b, with the range $\beta_\infty < \beta < \beta_b$ called the wall-stabilised region. In practice, the vessel wall has a finite resistivity. Thus, on the time scale required for eddy currents to decay resistively, the magnetic perturbation of the external kink mode can penetrate the wall and so wall-stabilisation is inhibited. Operation above the no-wall beta limit is important in advanced tokamak regimes, which aim at steady-state operation with high plasma pressure and a large fraction of non-inductive bootstrap current. However, advanced scenarios are particularly susceptible to the pressure-driven kink mode due to broad current profiles and the associated low no-wall beta limits. Hence, it will probably be necessary to operate these scenarios in the wall-stabilised regime in order to achieve economically-attractive plasma performance.

Various experiments have shown that the RWM can be stabilised in such a way that the plasma can operate above the no-wall beta limit in the presence of rotation generated by unidirectional Neutral Beam Injection (NBI) [1–7]. The critical rotation at which the RWM was able to grow has been estimated by braking the plasma by applying non-axisymmetric magnetic fields. Such magnetic braking experiments have indicated that RWM stability requires the toroidal plasma rotation to be of the order of a few percent of the Alfv´en velocity [6,8]. However, the application of non-axisymmetric magnetic fields to brake the plasma can also partially drive the RWM [9]. More recent experiments with nearly balanced NBI [10–12] have found a critical velocity well below that found in the magnetic braking experiments. Furthermore, preliminary results from NSTX suggest that operation above the no-wall limit can be attained even with no plasma rotation at the resonant–$q = 2$ surface [13]. Hence, it is important to understand the stabilisation mechanism, especially

given that the rotation in ITER is uncertain and predicted to be relatively low [14]. Various models have been presented to explain the RWM damping due to kinetic effects relative to the particle motion. For instance, RWM stabilisation has been attributed to sound-wave damping [15], ion Landau damping [16], or more recently, precessional drift resonance with the trapped thermal ions [17, 18].

In order to assess the role of these kinetic effects in damping the RWM, the driftkinetic particle-following Hagis code [19] has been used to calculate the change in the potential energy of the kink mode in the presence of both trapped and passing ions. The code can be used in a perturbative manner to study kinetic resonance damping effects by diagnosing which particles cause the strongest wave-particle interactions. Whilst this gives an exact treatment of the kinetic effects, it does not self-consistently evolve the eigenmode structure in the presence of the particles, which has been shown to affect the RWM stability [20].

A weakly damped mode, such as the RWM in the presence of rotation or kinetic damping, can amplify the resonant component of magnetic field asymmetries [21]. One way to probe RWM stability experimentally is to examine the plasma response to externally applied non-axisymmetric magnetic fields. When the plasma pressure exceeds the no-wall β-limit, strong Resonant Field Amplification (RFA) occurs. The measured frequency spectrum of the RFA to externally applied rotating magnetic fields has been described by a single-mode approach [22]. This allows an absolute measurement of the damping rate and natural mode rotation frequency of the RWM.

In this paper, we first outline a model for determining the stability of the RWM from the resonant field amplification measurements, which includes the plasma response. Experimental measurments of the RFA in JET are presented in section 3, and the results are compared with our model. In section 4 the kinetic resonance damping effects on the external kink mode are considered for a typical JET discharge. The kinetic effects upon the growth rate of the RWM in JET plasmas is assessed in section 5 and compared to the RFA fitting model. Finally, conclusions and implications for RWM stability are discussed in section 6.

2. RESONANT FIELD AMPLIFICATION MODELS

The resonant field amplification amplitude is usually defined as the ratio of the plasma response to the externally applied field, B_r^{ext}. It can be found by measuring the perturbated radial magnetic field at the wall, B_r, so

$$A_{RFA} = \frac{B_r(r = r_{sensor}) - B_r^{ext}}{B_r^{ext}} \quad (1)$$

The resonant field amplification, A_{RFA}, is a complex number, whose phase angle refers to the toroidal phase of the plasma response with respect to the externally applied field [22]. The normal mode approach [23,24] predicts that the interaction of the RWM with the applied fields is well described by a system model for the evolution of the perturbed resonant field at the wall. In the presence of an applied field with angular frequency !ext, the single-mode model employed in reference [22] gives

$$A_{RFA} = c_s \frac{1 + \gamma_0 \tau_w)}{i w_{ext} \tau_w - \gamma_0 \tau_w} \tag{2}$$

where γ_0 is the growth rate of the RWM in the absence of any external perturbations, τ_W is the resistive diffusion time for wall currents and c_S is the ratio of the resonant component of the applied field to the applied field detected by the sensors at the wall.

Whilst this empirical model agrees quantitatively well with the RFA data from experiments in DIII-D [22], it is possible to include the plasma response to the applied fields more rigorously, following a similar approach as in reference [25]. In a cylindrical equilibrium surrounded by a resistive wall, the dispersion relation for the resistive wall mode takes the form [26, 27]

$$\Delta_s(p) = \frac{\Delta'_\infty (1 + \lambda \Delta'_0 \Delta_w(p))}{1 + \lambda \Delta'_\infty \Delta_w(p)} \tag{3}$$

where Δ'_∞ and Δ'_0 are the stability indices for the case with a perfect wall at the location of the real resistive wall and without a conducting wall respectively. Δ_s and Δ_w are the jumps across the resonant surface inside the plasma and across the resistive wall respectively, and both are functions of the complex growth rate, p.

Now consider the case when a magnetic field is applied by a coil carrying a current, I_c, just inside a thick resistive wall at radius b and the perturbation is measured by a detector positioned at a thin resistive wall at radius a. Assuming a vacuum, the flux function, $\psi = rB_r$, is given by

$$\psi = B\left(\frac{r}{b}\right)^m + C\left(\frac{r}{b}\right)^{-m} \quad a < r < b \tag{4}$$

$$\psi = DK_m(\lambda r) \qquad b < r < \infty \tag{5}$$

where B, C and D are constants. Here m is the poloidal mode number, $\lambda^2 = p/\eta_b$, η_b is the thick wall resistivity and K_m is a modified Bessel function [28] defined in terms of Kelvin functions as $K_m(xe^{i\pi/4}) = e^{im\pi/2}[ker_m(x) + ikei_m(x)]$. The continuity of the flux function and the jump in its derivative [29] at the thin resistive wall, r = a, lead to

$$\psi_a = B\sigma + C/\sigma \tag{6}$$

$$p\tau_a\psi_a = m(B\sigma + C/\sigma) - a\psi'_{a-} \tag{7}$$

where $\tau_a = a\delta w/\eta_a$, η_a is the thin wall resistivity and $\sigma = (a/b)^m$. At r = b the continuity condition and the presence of the coil current I_C [30] give

$$B + C = DK_m(z) \tag{8}$$

$$-imI_c b = DzK_m' - m(B-C) \tag{9}$$

where z = λb. Linear combinations of equations 6 and 7 give

$$2mB = a\ '_{a-} + \ _a(p\ _a + m) \tag{10}$$

$$-2mC/\sigma = a\psi'_{a-} + \psi_a(p\tau_a - m) \tag{11}$$

Substituting equations 10 and 11 into equations 8 and 9 leaves us with

$$DK_m = \frac{a\psi'_{a-}}{2m\sigma}(1-\sigma^2) + \frac{\psi_a}{2m\sigma}\left[m(1+\sigma^2) + \tau_a(1-\sigma^2)\right] \tag{12}$$

$$-DzK_{m-1} = -imI_c b + \frac{a\psi'_{a-}}{\sigma} + \frac{\psi_a}{\sigma}(\ \tau_a\ 1-m) \tag{13}$$

where we have used the recurrence relationship that $zK'_m + mK_m = -zK_{m-1}$ [28]. Finally eliminating D gives

$$\begin{aligned}\frac{imI_c b\sigma}{\psi_a} = a\frac{\psi'_{a-}}{\psi_a}\left[1 + \frac{(1-\sigma^2)zK_{m-1}}{2mK_m}\right] + m\left[1 + \frac{(1-\sigma^2)zK_{m-1}}{2mK_m}\right] + \\ + p\tau_a\left[1 + \frac{(1-\sigma^2)zK_{m-1}}{2mK_m}\right]\end{aligned} \tag{14}$$

Next we consider the RWM stability as measured by the stability index Δ′s at the resonant surface, s,

$$\frac{\Delta'_s}{r_s} = \frac{\psi'_{s+} - \psi'_{s-}}{\psi_s} \tag{15}$$

where ψ_{s-} and ψ_{s+} are the values of the flux function in the limit approaching the resonant surface from the inside and outside respectively. Using the generic relationships [29] that $\psi_{s+} = \alpha_1\psi_{a-} + \alpha_2\psi'_{a-}$, $r_s\psi'_{s+} = \alpha_3\psi_{a-} + \alpha_4\psi'_{a-}$ and $r_s\psi'_{s-}/\psi_s = c$, we have that

$$\Delta'_s = \frac{1 + \alpha_1\left(\frac{a\psi'_{a-}}{\psi_a}\right)}{\alpha_2 + \alpha_3\left(\frac{a\psi'_{a-}}{\psi_a}\right)} \tag{16}$$

When no current is applied to the external coils and in the absence of a wall (ie $\eta_w \to \infty$, $a\psi'_{a-}/\psi_a \to -m$), equation 16 gives $\psi'_0 \to (1-m\alpha_1)/(\alpha_2 - m\alpha_3)$, whereas in the perfect wall limit ($\psi_a \to 0$), $\Delta'_\infty - \alpha_1/\alpha_3$. Combining these limits with equation 16 gives us

$$\frac{a\psi'_{a-}}{\psi_a} = \frac{(\Delta'_0 - \Delta'_s) - m\alpha_3\Delta'_s\ (\Delta'_0 - \Delta'\ )}{{}_3\Delta'_0\,(\Delta'_s - \Delta'\ )} \tag{17}$$

which can be written as

$$\frac{a\ \dot{a}_-}{a} = X - m \tag{18}$$

where

$$\frac{a\psi_{a-}}{\psi_a} = \frac{(\Delta_s' - \Delta_0')}{(\Delta_s' - \Delta')}\left[m\frac{\Delta'}{\Delta_0'} - \frac{1}{\alpha_3\Delta_0'}\right] \tag{19}$$

Now we recast equation 14 in the form

$$\frac{a\ \dot{a}_-}{a} + C_1 = \frac{C_2}{a} \tag{20}$$

Since, in the vacuum case $a\psi'_{a-}/\psi_a = m$, equation 20 yields

$$\frac{a}{a^{vac}} = \frac{m + C_2}{a_-/\ a + C_1} \tag{21}$$

Recasting equation 1 as $A_{RFA} = (\psi_w - \psi_w^{vac})/\psi_w^{vac}$, substituting in C_1 defined through equation 14 and assuming that the applied frequency, ω_{ext}, is much larger than the growth rate of the mode (which is typically the case in the RFA experiments in JET) yields

$$A_{RFA} = \frac{2m - X}{iw_{ext}\ a + X + \frac{2mzo^2K_{m-1}}{2mK_m + (1-o^2)zK_{m-1}}} \tag{22}$$

where we recall that $z = z(\omega_{ext}, \tau_b)$. This results in a two-parameter (namely, the real and imaginary parts of X) model which can be employed to estimate the stability parameter, Δ'_s of the RWM from the RFA measured experimentally. Note that there is an additional parameter, α_3, but since the second term in square brackets in equation 19 is an order of magnitude smaller than the first, the model can be considered independent of α_3. The benefit of using this scheme is that the information about the no-wall and with-wall beta limits is retained, exemplified by the presence of Δ'_∞ and Δ'_0 stability parameters in equation 19. Consequently, this model potentially offers greater insight into the plasma response to the applied fields.

3. RESONANT FIELD AMPLIFICATION IN JET

In JET, oscillating non-axisymmetric magnetic fields can be applied using the Error Field Correction Coils (EFCCs), which consist of four coils arranged symmetrically around the outside of the vacuum vessel, each spanning 70^o toroidally [31]. The coils are located in octants 1, 3, 5 and 7 of the vessel, with toroidally opposite coils having oppositely directed currents to produce an odd-n spectrum. The plasma response is detected using six saddle coils, with a pair above, below and on the midplane respectively. The plasma response to the magnetic perturbation is calculated by comparing with

measurements of the externally applied field in a vacuum.

In these JET experiments, the external field is applied in H-mode discharges which reach $\beta_N \sim 3.5$. The plasma parameters are fixed as $I_p = 1.1$MA, $B_T = 1.35$T, $\bar{n}_e \sim 2.5\times10^{19}$m^{-3} with NBI power, $P_{NBI} \leq 20$MW. The large NBI power raises the plasma pressure above the no-wall limit found from ideal MHD stability calculations performed with the Mishka-1 code [32]. The external field is applied in identical discharges with a frequency of 3Hz, 6Hz or 10Hz either co- or counter- to the direction of plasma rotation. During each discharge the neutral beam power injected is increased so that β_N is increased and the plasma response is measured for different values of the plasma pressure. Figure 1 shows the evolution of β_N in JET Pulse No: 68962 as P_{NBI} increases. The toroidal rotation also increases, keeping the RWM stable throughout. By measuring the plasma response using the saddle coils, the amplitude of the resonant field amplification can be found according to equation 1

Experimentally the RFA is determined as a ratio of signals from combinations of orthogonal saddle loops, from Octants 1-5 and Octants 3-7 (EFCCs in Octants 3-7 were used in this case), which is close to the total RFA defined by equation 1 at N values below or close to the no-wall limit [33]. The RFA varies with the frequency of the applied field, as illustrated in figures 2 and 3. The dependence of the RFA amplitude with respect to the frequency of the applied field has been fitted to the predicted onepole form given by equation 2 [22] (figure 2) as well as our parametric plasma response model given by equation 22, as shown in figure 3. Here we use vacuum response data to find that the thin wall time is $\tau_a = 13.6$ms and the thick wall time is $\tau_b = 280$ms when a = 1.5 and b = 2.5. We arbitrarily set the parameter $\alpha_3 = 1$ (although the fit is rather insensitive to α_3). Whilst the thick wall model outlined in section 2 is not geometrically representative of the JET vacuum vessel and support structures, it does provide a good fit with vacuum data which cannot be obtained with a model using two thin walls between the EFCC and the plasma.

Figure 2 shows that the magnitude of the plasma response peaks with an applied field rotating at 2-4Hz. Whilst the magnitude of the plasma response in figure 2 increases with β_N, the frequency at which the RFA is maximised remains constant, in good agreement with results from DIII-D [22]. These experimental data fit the parameterisations reasonably well, especially at low β_N. The value of c_s from the parameterisation in equation 2 is approximately constant, since this depends upon the location of the sensors relative to the mode (as well as other equilibrium factors). When the RFA is fitted to equation 22, the stability parameter can be found by employing equation 19 and supplying Δ'_0 and Δ'_∞ scaled according to the growth rate of the perturbation calculated by ideal MHD simulations [29], $\Delta'_{\infty,0} \sim -\pi/\gamma_{\infty,0}\tau_A$, where $\tau_A = R_0/v_A$, the Alfvén speed $v_A = B_\phi/\sqrt{\rho\mu_0}$ and ρ is the mass density. This demonstrates how this parameterisation for the RFA can be used to ascertain information about the RWM stability limit. A comparison between the JET data and the kinetic damping modelling is given in section 5.

4. ASSESSMENT OF KINETIC DAMPING

Recent experiments [10–13] have shown that tokamak plasmas can be sustained above the no-wall

limit, even when the toroidal rotation is small. There is naturally much interest in understanding the passive stabilisation occurring from kinetic effects which is thought to underlie these results. The earliest models for kinetic damping of the RWM were based upon parallel viscosity or sound wave damping of the mode [15,34]. Later it was suggested that the RWM would be damped due to a resonance between the mode frequency and the transit (bounce) frequency of the passing (trapped) energetic ions in the plasma [16]. More recently, kinetic theory has also been applied to suggest that the RWM will be damped in the presence of trapped thermal ions due to a resonance between the mode and the drift precessional motion of the particles [17,18]. Hence, it is interesting to model the contribution to RWM stability from all the species of particles to ascertain which of these effects contribute to mode damping, and whether such kinetic damping significantly alters the limit.

The growth rate of the RWM can be formulated in terms of the MHD perturbed energy, as [35]

$$\gamma_w = -\frac{\delta W_\infty}{\delta W_b} \tag{23}$$

where $\delta W_{b,\infty}$ represents the sum of the plasma and vacuum energy with and without a wall respectively. Equation 23 can be extended to include the kinetic contribution to the plasma energy, δW_K, for low-frequency modes [18], such that

$$\gamma_w = -\frac{\delta W_\infty + \delta W_k}{\delta W_b + \delta W_k} \tag{24}$$

where $\delta W_\infty < 0$ and $\delta W_b > 0$, indicating that the plasma is in the region where the ideal external kink mode is stable, but the RWM is MHD unstable. Here, the Hagis drift kinetic code [19] is used to compute the change in the potential energy of the kink mode in the presence of a population of thermal and energetic particles, δW_K. Hagis is a particle-orbit code following the guiding centre motion of the particles. Consequently it includes any finite orbit width effects which have been neglected in previous studies [18]. The kinetic terms are evaluated using the with-wall marginally stable eigenfunction, which represents the best approximation of the actual RWM eigenfunction.

There has been significant recent progress in establishing high β_N regimes in JET [36,37]. The JET plasmas analysed here are above the no-wall limit with respect to the ideal external kink mode, as indicated in figure 4. For Pulse No: 68875 at t = 5.0s, the no-wall limit is found to be $\delta_N = 2.7$. Experimentally, JET Pulse No: 68875 reached N = 3.1 although the RFA occurs at a much lower pressure, as seen in figure 5, where the RFA in Pulse No: 68875 is compared with two other identical pulses. In each of these discharges the RFA limit seems to agree well with the calculated no-wall limit. However, it should be noted that the δ-limits cannot be firmly ascertained because of the uncertainty in the current profile, most notably the edge current density [33]. The static eigenfunction is computed using the Mishka-1 code [32] for the no-wall case, and then input into Hagis together with the equilibrium generated by the Helena code [38]. The equilibrium is reconstructed by taking the plasma shape and current density profile from the Efit equilibrium code [39] together with the

thermal pressure profile obtained from the LIDAR diagnostic, and assuming that $p_i = p_e$. The q-profile is constrained by matching the frequency of MHD modes in the plasma to the rotation measured by the Charge Exchange diagnostic, and inferring the radial location of the resonant surfaces from the rotation profile. The charge exchange recombination spectroscopy measures the rotation of C_6^+ ions, though the correction to deuterium is expected to be small. Figure 6 shows the q-profile generated, together with the radial location of the 3/2 and 5/3 resonant surfaces. When the RWM stability in JET Pulse No: 68875 is assessed with an ideal wall at the position of the actual JET vacuum vessel with respect to the plasma, the β-limit is found to be $\beta_N^b = 2.9$. However, the plasma reaches values above this limit experimentally, implying that either the RWM stability is significantly affected by the metal structures that support the limiter tiles and are electrically closed to the vaccum vessel or that the equilibrium profiles are inaccurate. Therefore, we also assess the mode stability when the wall boundary is taken as that of the vacuum vessel modified to form a closed path around any brackets and restraint rings that are grounded to the vessel. Using this optimised wall, the β_N-limit is increased to $\beta_N^b = 3.95$. This assumes that the wall is axisymmetric, when in reality a full three-dimensional geometry is required. In order to show the sensitivity of the modelling to the wall location, we also consider a case with the wall taken between the vacuum vessel and the optimised geometry including support structures, equivalent to a conformal wall position at r = 1.3a. This produces a β-limit of $\beta_N^b = 3.7$. This arbitrary wall position is justified by the fact that this wall position gives a with wall limit of $\beta_N^b = 3.9$ for JET Pulse No: 62650, which agrees well with the plasma pressure achieved in the experiment before an MHD instability limited plasma performance [40]. Full three-dimensional modelling of the JET wall using the CarMa code [41, 42] will appear elsewhere. It should be noted that Mishka-1 does not include a resistive wall, so the eigenfunction used in the kinetic calculations is that of an ideal external kink mode, as shown in figure 7. This perturbative method does not allow for changes to the eigenfunction due to the presence of the resonant particles, which has been shown to somewhat alter the stability boundary including kinetic damping [20, 43]. Nonetheless, the analysis presented here gives a qualitative assessment of the kinetic damping, and importantly treats the wave-particle interaction rigorously without assumption.

Assuming that the equilibrium pressure goes to zero at the plasma edge, then the change in the potential energy of the kink mode can be calculated as [44, 45]

$$\delta W_k = \frac{1}{2}\int d\Gamma (m v_{\|} + \mu B)\delta f \sum \kappa \cdot \xi^{(m)*}(r, t) e^{-i(n-m)} \tag{25}$$

where ϕ is the toroidal angle, θ is the poloidal angle, $\boldsymbol{k} = \mathbf{b} \cdot \nabla \mathbf{b}$ is the curvature vector, $\boldsymbol{b} = \boldsymbol{b}/B$ and δf is the perturbed distribution function. Analytic theory developed for large aspect ratio circular plasmas shows that the contribution from the perturbed distribution function, found by solving the drift kinetic equation, leads to a kinetic potential energy of the form

$$\delta W_k \sim \sum_{l=-} \frac{w - n\Omega - n w_*}{w - n\Omega - n\langle \phi_E \rangle_{md} - l\langle \dot{\theta} \rangle} \tag{26}$$

where ω is the mode frequency, Ω is the plasma rotation frequency, ϕ_E has been redefined to be in a frame rotating with the **E**×**B** velocity, the dots represent the time derivative and $\langle ... \rangle$ is the orbit average, $\langle \dot{\phi}_E \rangle_{md} = \langle \dot{\phi}_E \rangle - \Omega_{E\times B}(r)$ and ω_* is the diamagnetic frequency,

$$w_{*i,e} = \frac{m_{i,e}}{Ze} \frac{\delta f_{i,e}/\delta\psi|_\varepsilon}{\delta f_{i,e}/\delta\varepsilon|_\psi} + \Omega_{E\times B} \tag{27}$$

where $\varepsilon = v^2/2$. When the toroidal and poloidal bounce(transit)-averaged frequencies are calculated, it is found that there are three regimes in which resonance can occur, that is to say, the magnitude of the denominator in equation 26 is minimised. Ignoring plasma rotation, these are when the mode frequency coincides with the transit frequency of passing particles, $\omega \approx \omega_t \sim (v_{th}/R)$; when the mode frequency is approximately the same as the bounce frequency of trapped particles, $\omega \approx \omega_b \sim \sqrt{r/R}(v_{th}/R)$; and when the mode frequency balances the precession drift motion, $\omega \approx \omega_d \sim \rho r(v_{th}/R)$, with $\omega_d << \omega_b < \omega_t$.

It is possible to use Hagis to calculate $\omega - n\Omega - n\langle\dot{\phi}_E\rangle - l\langle\dot{\theta}\rangle$ for a population of markers spread evenly across phase space. The distribution function of thermal ions and electrons is assumed to be isotropic in pitch angle and Maxwellian in energy whereas the energetic ions are given by the distribution function generated by the Transp transport code [46]. Figure 8 shows the contribution from these markers to the change in the mode energy as a function of pitch angle $\lambda = v_{||}/v$ and energy. Here the markers are evolved in the presence of a perturbation with frequency, $\tilde{\omega} = 10$kHz. The lines of resonance are shown by plotting the magnitude of $1/(\omega - n\tilde{\omega}_{\phi E} - l\omega_\theta)$ on a logarithmic scale, where $\tilde{\omega} = \omega - n\Omega$ is the Doppler-shifted mode frequency. The areas of strongest interaction indicate that the particles in that region of phase space have appropriate toroidal and poloidal frequencies to maximise equation 26. In the presence of very small rotation, only the precession drift of the particles can contribute, which happens when the quantum number $l = 0$. This limit is appropriate for the passive stabilising effect on the RWM exhibited experimentally in very slowly rotating plasmas. It should be noted that the drift precession frequency may be larger in the NSTX experiments since $\omega_d \sim q/R_0B_0$, so a larger mode frequency would be required for resonance to occur. When the plasma frequency is increased more lines of resonance appear in phase space since more particles are moving with appropriate bounce/transit frequencies.

Furthermore, it is also possible to examine where the strongest interaction between the particles and the kink mode occurs. Figure 9 shows the change in the mode energy due to the particles as a function of radius, where for each data point the markers were only loaded in a narrow radial region, $\Delta r = 0.1a$, where a is the plasma minor radius. It is clear that the strongest wave-particle interaction occurs when the particles are born at mid-radius. Since only thermal particles are considered here, the orbit widths are small compared to the radial bins. It should be noted that in Hagis, when a particle orbit reaches the separatrix, the particle is considered as lost. This means that the role of particles near the plasma edge may be underestimated.

It is also of interest to consider the interaction arising from the precessional drift resonance of

the trapped thermal ions as the plasma rotation frequency varies. Figure 10 shows δW_K as a function of Ω for JET Pulse No: 68875. The thermal particle distribution function is considered to be isotropic with respect to pitch angle and Maxwellian with respect to energy. Evidently, the plasma rotation plays a significant role in determining the kinetic stabilising effect upon the mode. The wave-particle interaction is strongest when the Doppler shifted mode frequency is approximately the same as the average precession drift frequency of the ensemble of trapped particles. As the rotation was decreased in the magnetic braking experiments in JET [8], as well as reducing the fluid stabilisation of the RWM caused by the flow shear, the rotation also reduced the stabilising effect arising from the resonance with the precessional motion of the trapped ions. With reducing plasma rotation frequency the stabilising contribution from the precessional drift resonance continues to decrease until some minimum, after which it suddenly increases once more. The implication of this is that if the toroidal rotation is reduced at a sufficiently low β_N that the weak rotation still present is able to stabilise the RWM, then β_N may be subsequently raised above β_∞, since the damping from the kinetic effects strongly increases at low rotation. This may partially explain how recent experiments have found the RWM stable at very low rotation when $\beta > \beta_\infty$ [10,11,13].

From equation 26 it is evident that the kinetic contribution to the stability of the RWM is also strongly determined by the magnitude of the diamagnetic frequency, $\omega_* = (Tdp/dr)/ZeBp$. Due to the strong pressure gradients present at the pedestal in H-mode plasmas, the diamagnetic frequency is large at the plasma edge, coincident with the dominant component of the RWM eigenfunction. Consequently, the kinetic damping of the RWM can be enhanced by the presence of strong pressure gradients at the plasma boundary. In the magnetic braking experiments performed on JET [8] and DIII-D [6], the application of external fields leads to a significant reduction in the edge density gradient [47, 48]. It has been suggested [10] that the anomalously high critical rotation for RWM onset found in these magnetic braking experiments was due to the applied error field amplifying the mode. However, it could also be envisaged that applying these non-axisymmetric magnetic fields also degrades the edge density gradient, so reducing the diamagnetic frequency, and subsequently reducing the kinetic damping of the RWM.

Figure 11 shows the change in the potential energy of the external kink mode in the presence of thermal particles when the pressure gradient is changed. The pressure profile is obtained from the Transp code, then the pedestal pressure gradient is artificially scaled by a Gaussian multiplication factor. For a reduction in the pressure gradient associated with a typical experimental reduction in density, δW_K is reduced by nearly 25%. It should be noted that the change in the edge pressure gradient is only one effect influencing the RWM; the change in the rotation profile from magnetic braking and the direct drive of the mode by error fields will also affect RWM stability.

5. MODELLING KINETIC DAMPING RATES IN JET

By using equation 24, the RWM growth rate can be found when the kinetic damping effects are included by calculating accurately δW_K due to both ions and electrons using Hagis. The MHD and

kinetic contributions to the mode energy have been calculated for JET Pulse No: 68875 for a Maxwellian isotropic population of thermal particles. The ideal no-wall limit is found to be β_∞ = 2.7, though the plasma reaches β_N values greater than this, up to β_N = 3.1. The contributions to the kink mode potential energy are shown in figure 12. The Mishka-1 MHD stability code cannot find δW_{MHD} with a wall when $\beta_N < \beta_b$. Therefore, the curve indicating MHD stability in the presence of a perfect wall has been extrapolated in order to find the RWM growth rate in the wall-stabilised region. The growth rate of the RWM, $\gamma\tau_W$, calculated using equation 24 is illustrated in figure 13. Including the kinetic effects increases the RWM stability limit by over 10%, beyond the no-wall limit.

Another comparison can be made between the RWM stability measured from the RFA experiments detailed in section 3 and the stability calculated by numerical modelling. In order to compare the kinetic damping modelling with the experimental data, we find the parameter X, as defined in equation 19, using two different methods. Firstly, X is found by fitting the JET RFA data according to equation 22. Secondly, we employ the visco-resistive model for the resistive wall mode [49], use $\Delta'_s = i/\Omega_{q=2}\tau_A$, and find $\Delta'_{\infty,0} = -\pi/\gamma_{\infty,0}\tau_A$, where the growth rates include the kinetic damping effects. In order to find $\gamma_{\infty,0}$, a β scan is performed by reconstructing JET Pulse No: 68962 early in the shot when β_N = 2.5 and scaling the plasma pressure in the Mishka-1 code. In this scan both the realistic geometrical representation of the JET wall (including the limiter support structures grounded to the vacuum vessel) is used (wall1), and the less optimistic case approximately equivalent to having a conformal wall at r = 1.3a (wall2) is also tested to illustrate the sensitivity of the results to the wall position. The comparison between the RFA data fitting and the kinetic damping modelling calculation of X is given in table 1.

The reasonable agreement between the experimental data and the kinetic modelling suggests that the damping of the RWM in JET is strongly influenced by the mode resonance with the precession motion of the thermal ions. For these JET plasmas, it can be diagnosed that the strongest contribution to δW_K arises due to the presence of a thermal population of particles. The drift precession frequency of a large number of these thermal particles is very similar to the Doppler-shifted mode frequency of the RWM, hence facilitating strong resonant damping. By examining the markers with the largest δf, the orbits and frequencies of the particles that incur the greatest kinetic damping of the mode can be obtained. Such a diagnosis has found that the strongest damping is from trapped particles with frequencies near the average precessional drift frequency. Whilst the stability calculated by our drift-kinetic modelling agrees reasonably well with the JET measurements, there remains some discrepancy. One reason for this could be that in the experiment the RWM experiences rotational damping which is not included in the modelling presented here. Also, the kinetic modelling uses a full toroidal geometry whereas the model presented in section 2 assumes cylindrical geometry, which alone could account for the ~20% difference in X. Furthermore, since the growth of the RWM is an inherently non-linear process, as the mode interacts with error fields, plasma rotation and the plasma particle populations, this linear modelling can only provide a qualitative insight into the mode stability. Nonetheless, this analysis does provide valuable information concerning which

species of plasma particles has the strongest influence in kinetically damping the mode, and by how much this kinetic damping can typically affect RWM stability. Non-linear MHD modelling including kinetic effects will be addressed in future studies.

CONCLUSIONS

The stability of the resistive wall mode in JET plasmas has been analysed by considering experimental measurments of the resonant field amplification and through modelling to assess the kinetic damping of the mode. The kinetic effects upon the RWM have been analysed for typical JET discharges using the Hagis drift-kinetic code. Hagis calculates the change in the potential energy of the mode due to the presence of both trapped and passing particles. By considering a range of energies and pitch angles, the particles which contribute most to the damping of the RWM have been diagnosed. It is found that the strongest kinetic damping arises due to the presence of trapped thermal particles, whose precessional drift frequency is similar to that of the RWM. Whilst stabilisation of the kink mode can occur due to resonance in other frequency regimes, for instance, at the transit or bounce frequencies, the very low mode frequency of the RWM dictates that more particles will interact with the mode at the precession drift frequency. The effects of equilibrium toroidal rotation and pressure gradients upon the kinetic damping of the RWM have also been considered. As the plasma rotation frequency varies, the kinetic stabilisation of the mode varies significantly. Together with the change in the kinetic contribution to mode stability at different edge pressure gradients, this may help to explain the different critical rotation for RWM onset found in experiments using magnetic braking compared with those using balanced neutral beam injection.

Also presented are results from JET showing the resonant field amplification of an oscillating applied field in the presence of a weakly damped RWM. Measurements of the RFA allow the application of parameter models to infer the stability of the RWM. A new fitting model is presented which allows the stability parameter of the RWM to be calculated from the RFA data, whilst retaining the information about the with-wall and no-wall β-limits. Consequently, this model potentially offers greater insight into the plasma response to the applied magnetic fields.

ACKNOWLEDGMENTS

This work was partly funded by the United Kingdom Engineering and Physical Sciences Research Council and by the European Communities under the contract of Association between EURATOM and UKAEA. The views and opinions expressed herein do not necessarily reflect those of the European Commission. This work was carried out within the framework of the European Fusion Development Agreement.

REFERENCES

[1]. Strait E.J. et al 1995 Phys. Rev. Lett. **74** 2483

[2]. Hender T.C. et al 2006 21st IAEA Fusion Energy Conference, Chengdu, China EX/P8-18

[3]. Sabbagh S.A. et al 2006 Nucl. Fusion **46** 635
[4]. Garofalo A.M. et al 1999 Phys. Rev. Letters **82** 3811
[5]. Garofalo A.M. et al 2002 Phys. Plasmas **9** 1997
[6]. La Haye R.J. et al 2004 Nucl. Fusion **44** 1197
[7]. Sontag A.C. et al 2005 Phys. Plasmas **12** 056112
[8]. Reimerdes H. et al 2006 Phys. Plasmas **13** 056107
[9]. Fitzpatrick R. and Hender T.C. 1991 Phys. Fluids **B3** 644
[10]. Reimerdes H. et al 2007 Phys. Rev. Lett. **93** 055001
[11]. Takechi M. et al 2007 Phys. Rev. Lett. **93** 055002
[12]. Strait E.J. et al 2007 Phys. Plasmas **14** 056101
[13]. Sabbagh S.A. et al 2008 22nd IAEA Fusion Energy Conference, Geneva, Switzerland EX/5-1
[14]. Rice J et al 2007 Nucl. Fusion **47** 1618
[15]. Bondeson A and Ward DJ 1994 Phys. Rev. Lett. **72** 2709
[16]. Chu MS et al 1995 Phys. Plasmas **2** 2236
[17]. Hu B., Betti R ,and Manickam J, 2005 Phys. Plasmas **12** 057301
[18]. Hu B., Betti R, 2004 Phys. Rev. Lett. **93** 105002
[19]. Pinches S.D. et al 1998 Comput. Phys. Commun. **111** 133 (Release Version 8.09)
[20]. Liu Y,Q, Chapman I,T,, Chu M,S, Gimblett C,G, Gryaznevich M.G, Hastie R.J, Hender T.C, Howell DF and Saarelma S, 2008 22nd IAEA Fusion Energy Conference, Geneva, Switzerland TH/P9-26
[21]. Boozer A.H. 2001 Phys. Rev. Lett. **86** 5059
[22]. Reimerdes H. et al 2004 Phys. Rev. Lett. **93** 135002
[23]. Garofalo A.M, Jensen T.H. and Strait E.J. 2002 Phys. Plasmas **9** 4573
[24]. Chu M.S. et al 2003 Nucl. Fusion **43** 196
[25]. Pustovitov V.D. 2004 Plasma Phys. Rep. **30** 187
[26]. Finn J.M. 1995 Phys. Plasmas **2** 198; 1995 Phys. Plasmas 2 3782
[27]. Fitzpatrick R. 2002 Phys. Plasmas **9** 3459
[28]. Abramowitz M. and Stegun A.I. 1965 Handbook of mathematical functions, with formulas, graphs and mathematical tables Dover Publications (New York) p374-379
[29]. Gimblett C.G, 1986 Nucl. Fusion **26** 617
[30]. Gimblett C.G and Hastie RJ 2004 Phys. Plasmas **11** 1019
[31]. Barlow I. et al 2001 Fusion Engineering and Design **58** 189
[32]. Mikhailovskii A.B, Huysmans G.T.A, Sharapov S.E. and Kerner WO 1997 Plasma Phys. Rep. 23 844
[33]. Gryaznevich M.P. et al 2008 Plasma Phys. Control. Fusion **50** 124030
[34]. Betti R. and Friedberg J.P. 1995 Phys. Rev. Lett. **74** 2429
[35]. Haney S.W. and Friedberg J.P. 1989 Phys. Fluids **B1** 1637
[36]. Litaudon X et al 2007 Phys. Plasmas Control. Fusion **49** B529

[37]. Rimini F.G et al, 2008 22nd IAEA Fusion Energy Conference, Geneva, Switzerland EX/1-2
[38]. Huysmans G, Goedbloed J and Kerner W. 1991 Proceedings of the CP90 Conference on Computer Physics, Amsterdam, (World Scientific, Singapore), p. 371
[39]. Lao L et al 1990 Nucl. Fusion **30** 1035
[40]. Hender T.C. et al 2004 20th IAEA Fusion Energy Conference, Vilamoura, Portugal EX/P2-22
[41]. Albanese R, Liu Y.Q, Portone A, Rubinacci G and Villone F, 2007, Proc. of 16th COMPUMAG Conference, Aachen, Germany
[42]. Portone A, Villone F, Liu YQ, Albanese R. and Rubinacci G, 2008 Plasma Phys. Control. Fusion **50** 085004
[43]. Liu Y.Q, Chapman I.T, Chu M.S. and Hender T.C, 2008 Phys Plasmas **15** 112503
[44]. Breizman B.N, Candy J, Porcelli F. and Berk H. 1998 Phys. Plasmas **5** 2326
[45]. Porcelli F. 1991 Plasma Phys. Control. Fusion **33** 1601
[46]. Budny R. et al 1992 Nucl. Fusion **32** 429
[47]. Liang Y. et al 2007 Phys. Rev. Lett. **98** 265004
[48]. Evans T.E. et al 2008 Nucl. Fusion **48** 024002
[49]. Fitzpatrick R. 1994 Phys. Plasmas **1** 3308

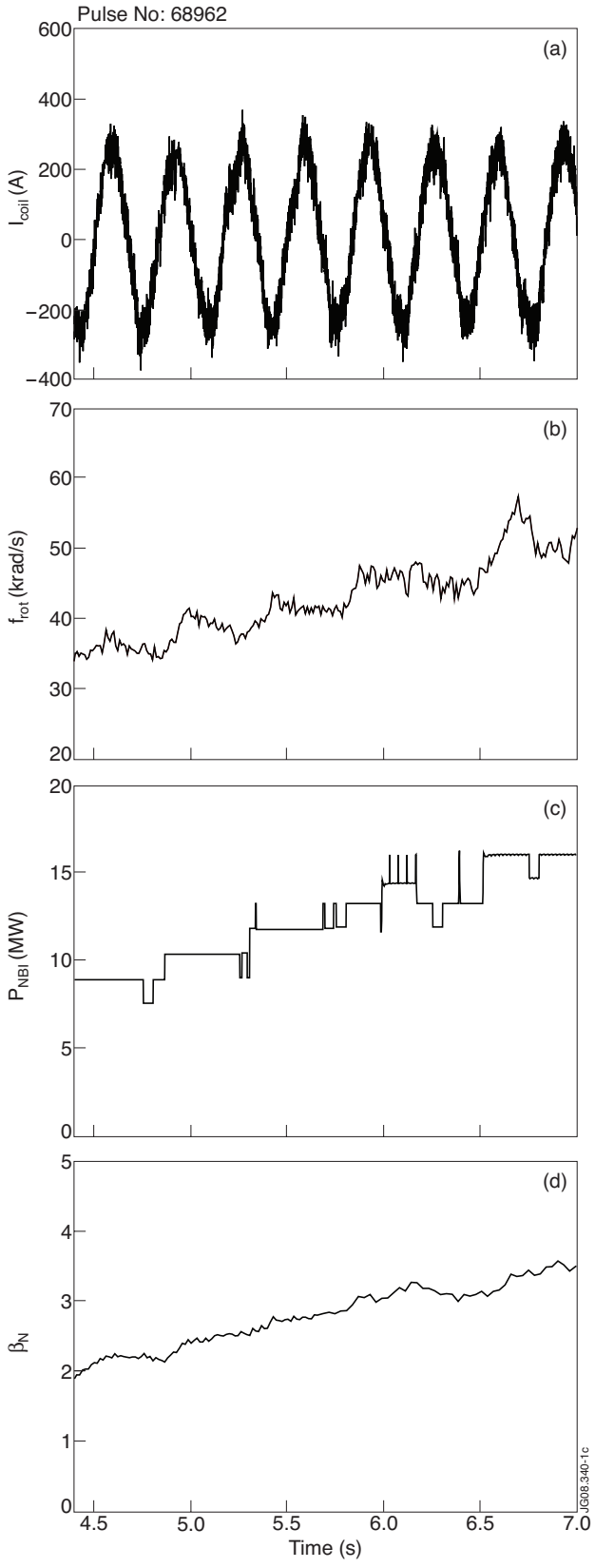

Figure 1: (a) The oscillating applied field in JET Pulse No: 68962. (b) The strong toroidal rotation at (c) increasing beam power means that the RWM is stable even at (d) high β_N.

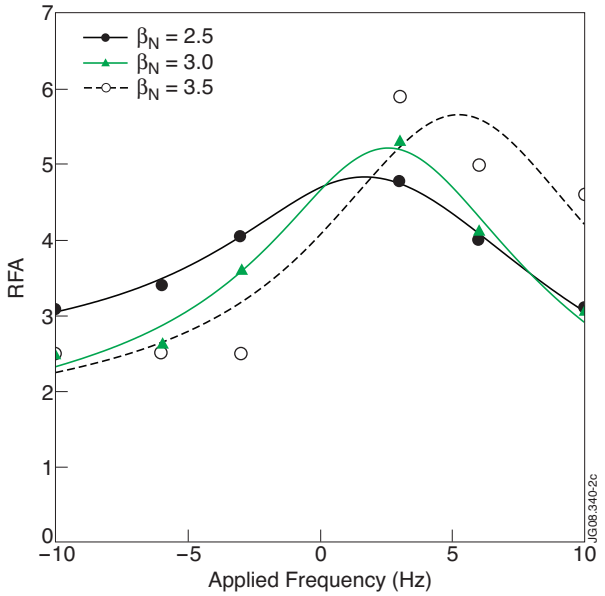

Figure 2: Magnitude of the n = 1 resonant field amplification in JET plasmas as a function of the frequency of the applied field, fitted to equation 2.

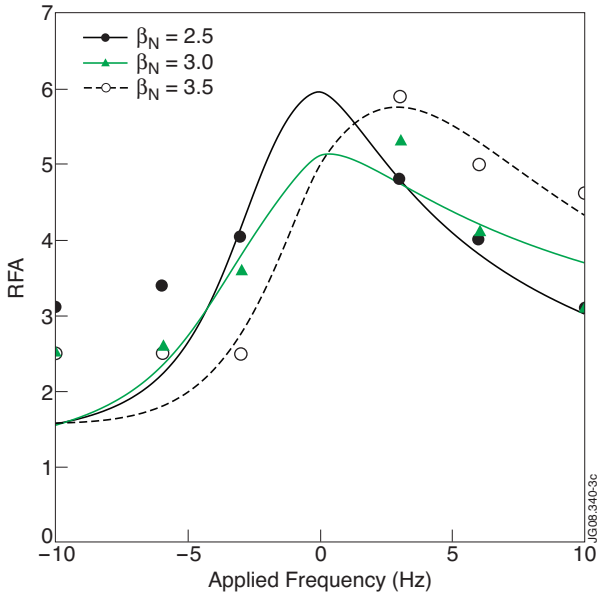

Figure 3: Magnitude of the n = 1 resonant field amplification in JET plasmas as a function of the frequency of the applied field, fitted to equation 22.

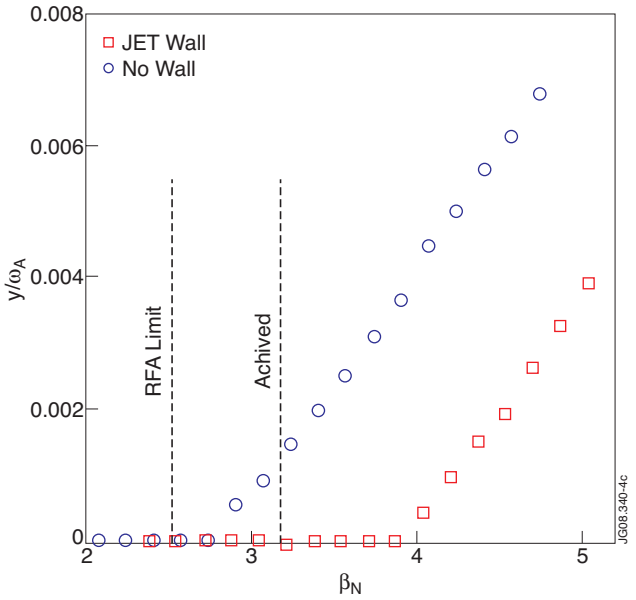

Figure 4. The fluid no-wall and with-wall β-limits for JET Pulse No: 68875 calculated using the Mishka-1 code with the JET vacuum vessel and support structures. Shown for comparison is the RFA threshold.

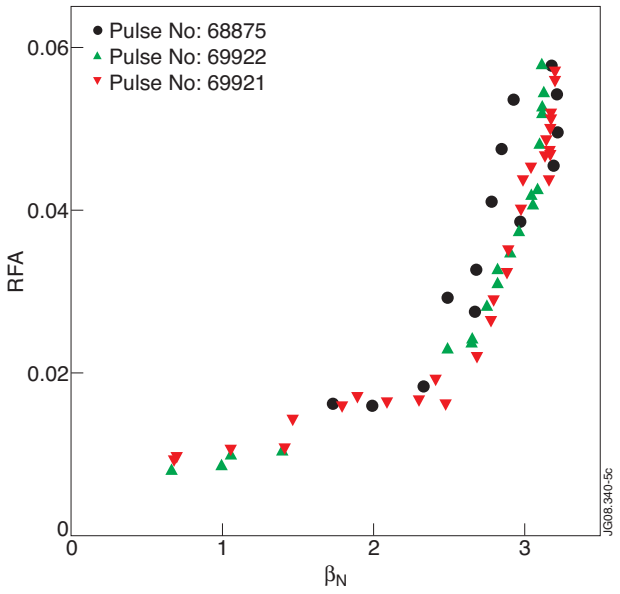

Figure 5. The RFA in JET Pulse No's: 68875, 69921 and 69922 as a function of β_N. The RFA limit is in broad agreement with the no-wall limit, $\beta_N^{\infty} = 2.7$.

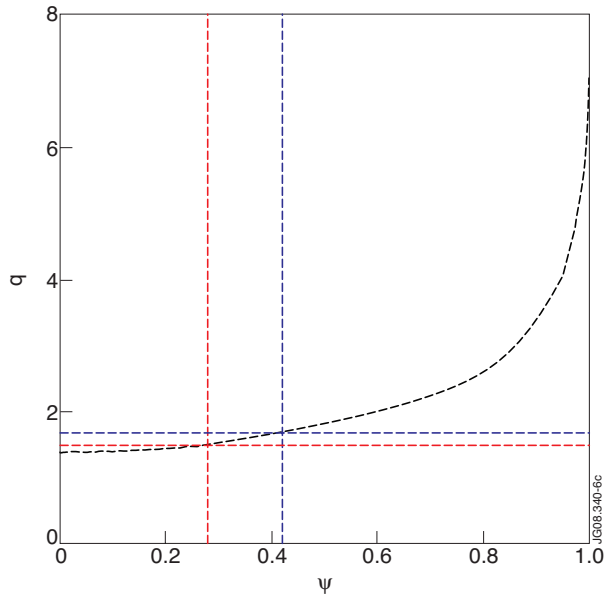

Figure 6: The q-profile for JET Pulse No: 68875 at t = 5s constrained by the location of MHD activity at resonant surfaces in the plasma.

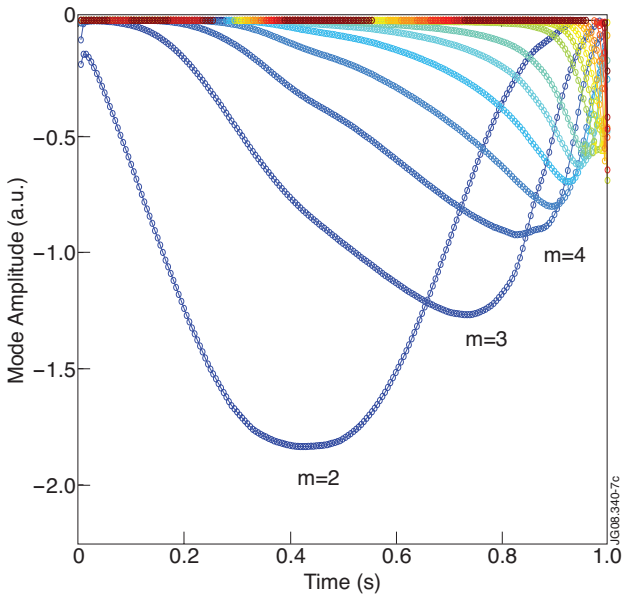

Figure 7: The eigenfunction for an unstable pressure-driven external kink mode in JET Pulse No: 68875.

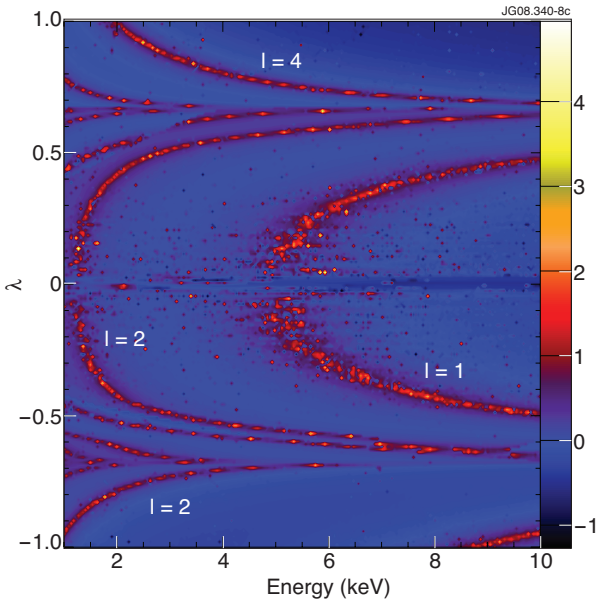

Figure 8: Lines of resonance in ε–λ phase space showing the dominant regions of wave-particle interaction, occurring when $\omega \approx \Omega + nh\langle\dot{\phi}_E\rangle + l\langle\dot{\theta}\rangle$.

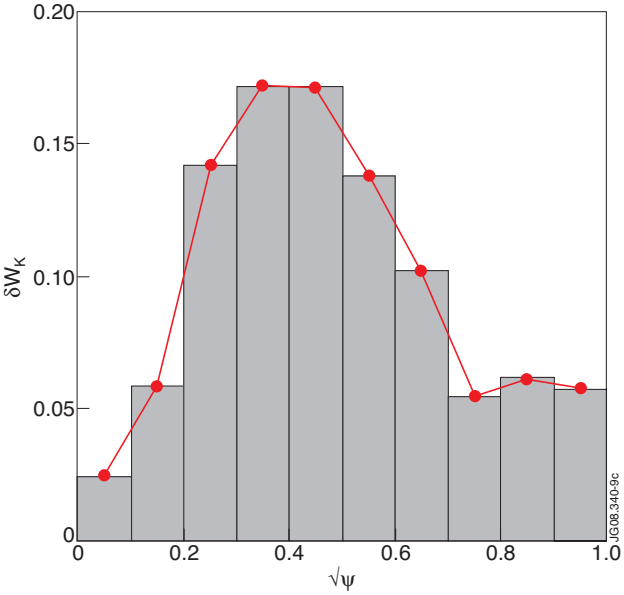

Figure 9: The radial location of the strongest wave-particle interaction. Note that whilst the eigenfunction is large near the edge, since most particles born near the separatrix are lost, the largest interaction is at mid-radius.

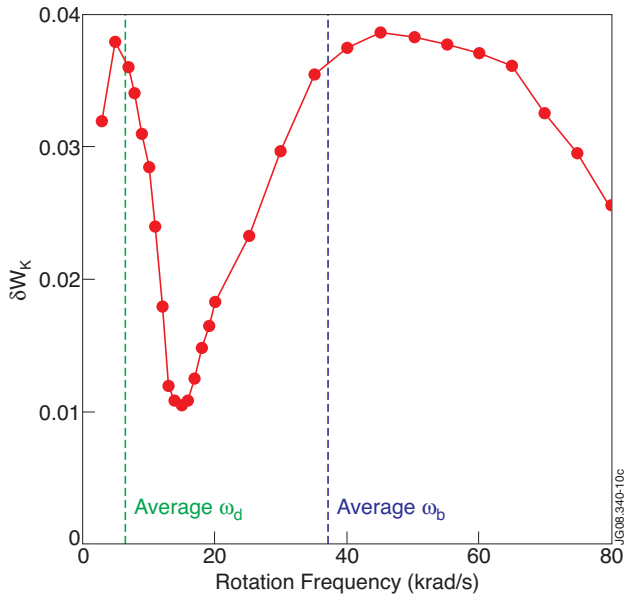

Figure 10: The real part of the change in the potential energy of the kink mode as a function of the plasma toroidal rotation. The influence of the kinetic damping changes significantly as the rotation varies.

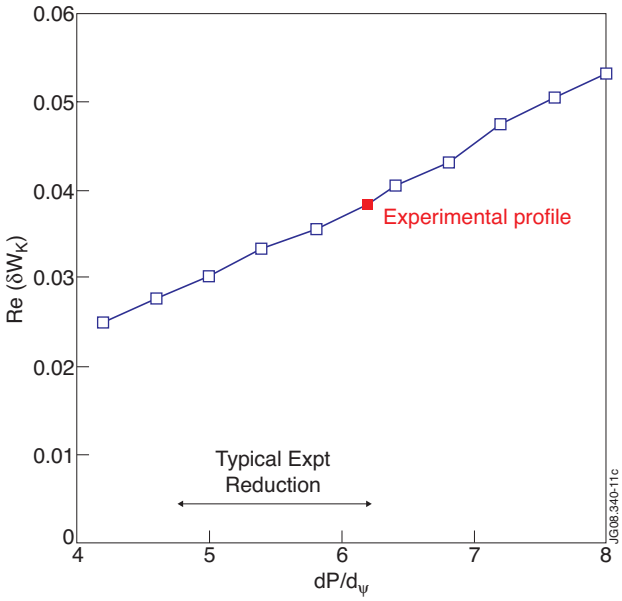

Figure 11: The real part of the kinetic contribution to the mode energy as a function of pressure gradient in the pedestal. Since δW_K depends upon the diamagnetic frequency, it is thus sensitive to the density gradient.

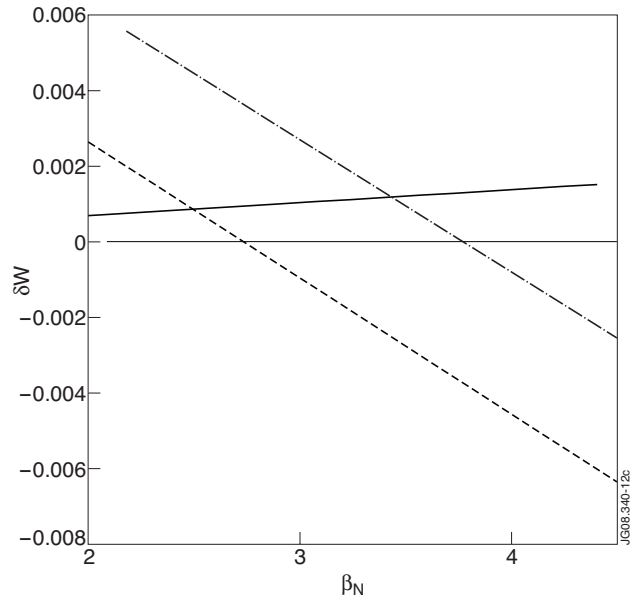

Figure 12. Contributions to the change in the potential energy of the kink mode from the MHD terms (with and without a wall) and the kinetic terms for JET Pulse No: 68875.

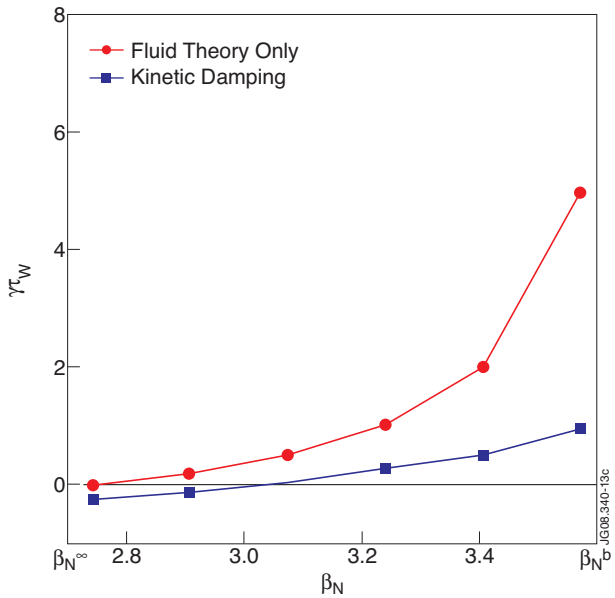

Figure 13. The β-limit of the RWM is increased by approximately 15% for JET Pulse No: 68875 when the kinetic damping terms are included.